

Unscented Particle Filter for Visual-inertial Navigation using IMU and Landmark Measurements

Khashayar Ghanizadegan and Hashim A. Hashim

Abstract—This paper introduces a geometric Quaternion-based Unscented Particle Filter for Visual-Inertial Navigation (QUPF-VIN) specifically designed for a vehicle operating with six degrees of freedom (6 DoF). The proposed QUPF-VIN technique is quaternion-based capturing the inherently nonlinear nature of true navigation kinematics. The filter fuses data from a low-cost inertial measurement unit (IMU) and landmark observations obtained via a vision sensor. The QUPF-VIN is implemented in discrete form to ensure seamless integration with onboard inertial sensing systems. Designed for robustness in GPS-denied environments, the proposed method has been validated through experiments with real-world dataset involving an unmanned aerial vehicle (UAV) equipped with a 6-axis IMU and a stereo camera, operating with 6 DoF. The numerical results demonstrate that the QUPF-VIN provides superior tracking accuracy compared to ground truth data. Additionally, a comparative analysis with a standard Kalman filter-based navigation technique further highlights the enhanced performance of the QUPF-VIN.

I. INTRODUCTION

ACCURATE navigation algorithms are crucial for autonomous ground and aerial vehicles, particularly in both indoor and outdoor applications where Global Positioning System (GPS) signals may be unavailable or unreliable. These techniques are essential for tasks such as warehouse management, surveillance, road and pipeline inspection, package delivery, and household robotics [1]–[3]. In such cases, GPS-independent navigation solutions become critical. In GPS-denied environments, autonomous vehicles rely on robust algorithms capable of providing reliable estimates using cost-effective inertial measurement units (IMUs). Navigation can be achieved with low-cost onboard sensors, such as 6-axis IMUs and either stereo or monocular cameras [1], [3]. A 6-axis IMU, comprising a gyroscope and accelerometer, provides measurements of a vehicle’s angular velocity and linear acceleration. Dead-reckoning, which has been extensively studied, is commonly used to estimate a vehicle’s navigation state (attitude (orientation), position, and linear velocity), while operating with six degrees of freedom (6 DoF) [1], [3]. This technique relies solely on IMU data, using numerical integration based on the vehicle’s initial state. However, dead-reckoning is prone to error accumulation, making it unsuitable for long-distance navigation [3]. Attitude-only estimation, on the other hand, can be reliably achieved through IMU measurements using robust

This work was supported in part by National Sciences and Engineering Research Council of Canada (NSERC), under the grants RGPIN-2022-04937 and DGECCR-2022-00103.

K. Ghanizadegan and H. A. Hashim are with the Department of Mechanical and Aerospace Engineering, Carleton University, Ottawa, Ontario, K1S-5B6, Canada (e-mail: hhashim@carleton.ca).

attitude filters, including deterministic filters [4] and stochastic approaches [3], [5], [6].

Pose estimation (attitude and position) of a vehicle navigating in three-dimensional (3D) space can be achieved through sensor fusion, such as the integration of landmark measurements from a vision system and data from an IMU. Commonly used filters for pose estimation include Kalman filters, the Extended Kalman Filter (EKF), and nonlinear filters [7], [8]. However, these algorithms typically require knowledge of the vehicle’s linear velocity, which poses a significant challenge in GPS-denied environments. In practice, uncertain attitude and position can be reconstructed through the fusion of vision data and IMU measurements [9]. Nevertheless, deriving or optimizing linear velocity from reconstructed uncertain attitude and position data proves impractical and unreliable. As a result, there is a growing demand for robust navigation techniques that can handle measurement uncertainties, provide accurate attitude and position estimates, and observe the vehicle’s linear velocity, which is often considered a hidden state [3]. True 6 DoF navigation kinematics are highly nonlinear [3], making linear filters inadequate for accurate navigation estimation [3], [10]. Kalman filters (KF) have been applied to vision-based navigation [11], with modifications such as the EKF [11] introduced to account for system nonlinearity. Further enhancements, like the Multiplicative EKF (MEKF) [2] and the Multi-State Constraint Kalman Filter (MSCKF) [12], were developed to improve accuracy and address consistency issues. Additionally, Unscented Kalman Filters (UKF) [13] have been proposed to better address the nonlinearity of kinematic models. However, the main limitation of KF is its disregard for navigation nonlinearities, while EKF linearizes the system around a nominal point. MEKF, MSCKF, and UKF rely on parametric statistical models that fail to capture the full complexity of arbitrary distributions in nonlinear navigation systems. The Particle Filter (PF) [14], which can capture arbitrary distributions, has been applied to navigation problems but struggles numerically when dealing with relatively accurate sensors. These sensors generate narrow distributions, causing particles to receive near-zero probabilities if they deviate slightly from the distribution’s peak, thus hindering effective guidance. The Unscented PF (UPF) [15] addresses this limitation by using UKF to propagate particles and estimate their mean and covariance, resulting in better alignment with the posterior distribution. This approach overcomes the shortcomings of PF when dealing with narrow distributions [15].

Contribution: This paper presents a geometric Quaternion-based Unscented Particle Filter for Visual-Inertial Navigation (QUPF-VIN) that relies on sensor data

TABLE I: Nomenclature

$\{\mathcal{B}\} / \{\mathcal{W}\}$:	Fixed body-frame / fixed world-frame
$\mathbb{SO}(3)$:	Special Orthogonal Group of order 3
\mathbb{S}^3	:	Three-unit-sphere
$\mathbb{R}^{n_1 \times n_2}$:	n_1 -by- n_2 real space
q_k, \hat{q}_k	:	True and estimated quaternion at step k
p_k, \hat{p}_k	:	True and estimated position at step k
v_k, \hat{v}_k	:	True and estimated linear velocity at step k
$r_{e,k}, p_{e,k}, v_{e,k}$:	Attitude, position, and velocity estimation error
$a_k, a_{m,k}$:	True and measured acceleration at step k
$\omega_k, \omega_{m,k}$:	True and measured angular velocity at step k
$n_{\omega,k}, n_{a,k}$:	Angular velocity and acceleration measurements noise
$b_{\omega,k}, b_{a,k}$:	Angular velocity and acceleration measurements bias
C_\times	:	Covariance matrix of \times .
f_b, f_w	:	landmark points coordinates in $\{\mathcal{B}\}$ and $\{\mathcal{W}\}$.
x_k, u_k	:	The state, and input vectors at the k th time step
z_k	:	True measurement
$\{\mathcal{X}_{k l}^{(i)}\},$ $\{\mathcal{X}_{k l}^{(i)a}\},$ $\{\mathcal{Z}_{k l}\}$:	Sigma points of state, augmented state, and measurements
$\{\mathcal{X}_k^{(i)}\}$:	Particles at step k

from a 6-axis IMU and landmark measurements. The proposed filter captures the nonlinear nature of navigation kinematics and is designed and implemented in a geometric discrete form at a low sampling rate. The effectiveness of QUPF-VIN is validated using a real-world quadrotor dataset, which includes low-cost IMU data and stereo images, and is compared against ground-truth data. The proposed navigation algorithm is suitable for implementation in both Unmanned Aerial Vehicles (UAVs) and ground vehicles.

Structure: The remainder of the paper is organized as follows: Section II discusses important math notation and preliminaries. Section III presents the true navigation kinematics and inertial measurement data (IMU and landmarks). Section IV introduces the QUPF-VIN, and steps of implementation. Section V illustrates the output performance of the proposed QUPF-VIN using a dataset obtained from real quadrotor flight and compares QUPF-VIN performance to a baseline filter. Finally, Section VI provides concluding remarks.

II. PRELIMINARY AND MATH NOTATION

The set of n_1 -by- n_2 real number matrices are described by $\mathbb{R}^{n_1 \times n_2}$. For a vector $x \in \mathbb{R}^{n_x}$, the Euclidean norm is denoted by $\|x\| = \sqrt{x^\top x} \in \mathbb{R}$. $\mathbf{I}_n \in \mathbb{R}^{n \times n}$ denotes an identity matrix. $\{\mathcal{W}\}$ describes the world-frame fixed to the Earth while $\{\mathcal{B}\}$ refers to the body-frame fixed to a moving vehicle. Table I lists a set of important symbols used subsequently. $[x]_\times$ denotes

skew-symmetric of $x \in \mathbb{R}^3$ such that

$$[x]_\times = \begin{bmatrix} 0 & -x_3 & x_2 \\ x_3 & 0 & -x_1 \\ -x_2 & x_1 & 0 \end{bmatrix} \in \mathfrak{so}(3), \quad x = \begin{bmatrix} x_1 \\ x_2 \\ x_3 \end{bmatrix} \quad (1)$$

$\text{vex}(\cdot)$ describes the inverse mapping where $\text{vex}([x]_\times) = x \in \mathbb{R}^3$. For $D \in \mathbb{R}^{3 \times 3}$, the anti-symmetric projection operator is given by:

$$\mathcal{P}_a(D) = \frac{1}{2}(D - D^\top) \in \mathfrak{so}(3) \quad (2)$$

Orientation of a vehicle is denoted by $R \in \mathbb{SO}(3)$ where $\mathbb{SO}(3)$ refers to the Special Orthogonal Group such that [16]:

$$\mathbb{SO}(3) := \{ R \in \mathbb{R}^{3 \times 3} \mid \det(R) = +1, R^\top R = \mathbf{I}_3 \} \quad (3)$$

Unit-quaternion $q = [q_w, q_x, q_y, q_z]^\top = [q_w, q_v^\top]^\top \in \mathbb{S}^3$ where $q_v \in \mathbb{R}^3$ and $q_w \in \mathbb{R}$ can be used to describe the vehicle's orientation where

$$\mathbb{S}^3 := \{ q \in \mathbb{R}^4 \mid \|q\| = 1 \} \quad (4)$$

and the vehicle's orientation is given by [16]:

$$R_q(q) = (q_w^2 - \|q_v\|^2)\mathbf{I}_3 + 2q_v q_v^\top + 2q_w [q_v]_\times \in \mathbb{SO}(3) \quad (5)$$

Define \otimes as quaternion product of two quaternions such that the quaternion product of $q_1 = [q_{w1}, q_{v1}]^\top \in \mathbb{S}^3$ and $q_2 = [q_{w2}, q_{v2}]^\top \in \mathbb{S}^3$ is [16]:

$$q_3 = q_1 \otimes q_2 = \begin{bmatrix} q_{w1}q_{w2} - q_{v1}^\top q_{v2} \\ q_{w1}q_{v2} + q_{w2}q_{v1} + [q_{v1}]_\times q_{v2} \end{bmatrix} \in \mathbb{S}^3 \quad (6)$$

and the inverse quaternion of $q = [q_w, q_v^\top]^\top \in \mathbb{S}^3$ is defined by $q^{-1} = [q_w, -q_v^\top]^\top \in \mathbb{S}^3$. $q_I = [1, 0, 0, 0]^\top$ describes the quaternion identity such that $q \otimes q^{-1} = q_I$. Angle-axis parameterization describes the orientation as a rotation (angle) $\alpha \in \mathbb{R}$ around a unit vector (axis) $v = [v_1, v_2, v_3] \in \mathbb{S}^2$ such that

$$r = r_{\alpha, v}(\alpha, v) = \alpha v \in \mathbb{R}^3 \quad (7)$$

where the rotation matrix corresponding to the angle-axis parameterization is defined by

$$\begin{aligned} R_r(r) &= \exp([r]_\times) \in \mathbb{SO}(3) \\ &= \mathbf{I}_3 + \sin(\alpha) [v]_\times + (1 - \cos(\alpha)) [v]_\times^2 \end{aligned} \quad (8)$$

Note that $\alpha_R = \arccos\left(\frac{\text{Tr}(R)-1}{2}\right) \in \mathbb{R}$ and $v_R = \frac{1}{\sin \alpha_R} \text{vex}(\mathcal{P}_a(R)) \in \mathbb{S}^2$ [16]. Using the rotation vector r in (7), one obtains

$$\begin{aligned} q_r(r) &= q_R(R_r(r)) \in \mathbb{S}^3 \\ &= [\cos(\alpha/2), \sin(\alpha/2)v^\top]^\top \in \mathbb{S}^3 \end{aligned} \quad (9)$$

with

$$r_q(q) = r_{\alpha, v}(\alpha_R(R_q(q)), v_R(R_q(q))) \in \mathbb{R}^3 \quad (10)$$

The following quaternion subtraction operator is defined:

$$q_1 \ominus q_2 := r_q(q_1 \otimes q_2^{-1}) \in \mathbb{R}^3, \quad \forall q_1, q_2 \in \mathbb{S}^3 \quad (11)$$

And the quaternion-rotation vector addition and subtraction operators are defined as:

$$q \oplus r := q_r(r) \otimes q \in \mathbb{S}^3, \quad \forall q \in \mathbb{S}^3, \forall r \in \mathbb{R}^3 \quad (12)$$

$$q \ominus r := q_r(r)^{-1} \otimes q \in \mathbb{S}^3, \quad \forall q \in \mathbb{S}^3, \forall r \in \mathbb{R}^3 \quad (13)$$

Consider $S = \{s_i\}$ to be scalar weights and let us define the following term:

$$D = \sum s_i q_i q_i^\top \in \mathbb{R}^{4 \times 4}$$

The unit eigenvector associated to eigenvalue with the highest magnitude can be obtained by:

$$\text{WM}(Q, W) = \text{EigVector}(D)_i \in \mathbb{S}^3 \quad (14)$$

where $i = \text{argmax}(|\text{EigValue}(D)_i|) \in \mathbb{R}$, $\text{WM}(D, W)$ denotes weighted mean, and $\text{EigValue}(D)_i$ refers to the i th eigenvalue of D . The Gaussian probability density function of a is defined as follows:

$$\begin{aligned} \mathbb{P}(a) &= \mathcal{N}(a | \bar{a}, P_a) \\ &= \frac{\exp(-\frac{1}{2}(a - \bar{a})^\top P_a^{-1}(a - \bar{a}))}{\sqrt{(2\pi)^n \det(P_a)}} \in \mathbb{R} \end{aligned}$$

where $a \in \mathbb{R}^n$ obtained through a Gaussian distribution $a \sim \mathcal{N}(\bar{a}, P_a)$, $\bar{a} \in \mathbb{R}^n$ denotes the mean of a , and $P_a \in \mathbb{R}^{n \times n}$ describes covariance matrix related to a .

III. PROBLEM FORMULATION AND SENSOR DATA

A. Navigation Model

Consider a vehicle travelling in 3D space where $\omega \in \mathbb{R}^3$ denotes its angular velocity and $a \in \mathbb{R}^3$ describes its acceleration measured with $\omega, a \in \{\mathcal{B}\}$. The vehicle's position and linear velocity are described by $p \in \mathbb{R}^3$ and $v \in \mathbb{R}^3$, respectively, where $p, v \in \{\mathcal{W}\}$, whereas the vehicle's orientation is described in view of quaternion $q \in \mathbb{S}^3$ and $q \in \{\mathcal{B}\}$. The navigation kinematics is described as follows [3], [17], [18]:

$$\begin{cases} \dot{q} = \frac{1}{2}\Gamma(\omega)q \in \mathbb{S}^3 \\ \dot{p} = v \in \mathbb{R}^3 \\ \dot{v} = g + R_q(q)a \in \mathbb{R}^3 \end{cases} \quad (15)$$

where

$$\Gamma(\omega) = \begin{bmatrix} 0 & -\omega^\top \\ \omega & -[\omega]_\times \end{bmatrix} \in \mathbb{R}^{4 \times 4}$$

and $g \in \{\mathcal{W}\}$ represents the gravitational acceleration vector. The Model in (15) can be re-formulated as follows:

$$\begin{bmatrix} \dot{q} \\ \dot{p} \\ \dot{v} \\ 0 \end{bmatrix} = \underbrace{\begin{bmatrix} \frac{1}{2}\Gamma(\omega)q & 0 & 0 & 0 \\ 0 & 0 & I_3 & 0 \\ 0 & 0 & 0 & g + R_q(q)a \\ 0 & 0 & 0 & 0 \end{bmatrix}}_{M^c(q, \omega, a)} \begin{bmatrix} q \\ p \\ v \\ 1 \end{bmatrix} \quad (16)$$

Since the sensor data operates and is collected in discrete space, the equation in (16) can be discretized for filter derivation and implementation. Let the subscript k of variable x_k refers to a sampled signal $x, p_k \in \mathbb{R}^3$ at the k th discrete time

step. The exact discretized system kinematics of (16) is given by:

$$\begin{bmatrix} q_k \\ p_k \\ v_k \\ 1 \end{bmatrix} = \exp(M_{k-1}^c dT) \begin{bmatrix} q_{k-1} \\ p_{k-1} \\ v_{k-1} \\ 1 \end{bmatrix} \quad (17)$$

with $M_{k-1}^c = M^c(q_{k-1}, \omega_{k-1}, a_{k-1})$ and dT being a sample time.

B. VIN Measurement Model

IMU data: Let $\omega_{m,k} \in \mathbb{R}^3$ and $a_{m,k} \in \mathbb{R}^3$ denotes the measured angular velocity and linear acceleration at k th time step, respectively, such that

$$\begin{cases} \omega_{m,k} = \omega_k + b_{\omega,k} + n_{\omega,k} \in \mathbb{R}^3 \\ a_{m,k} = a_k + b_{a,k} + n_{a,k} \in \mathbb{R}^3 \\ b_{\omega,k} = b_{\omega,k-1} + n_{b\omega,k-1} \in \mathbb{R}^3 \\ b_{a,k} = b_{a,k-1} + n_{ba,k-1} \in \mathbb{R}^3 \end{cases} \quad (18)$$

where $b_{\omega,k}$ denotes angular velocity bias and $b_{a,k}$ denotes linear acceleration bias. $n_{\omega,k} \in \mathbb{R}^3$, $n_{b\omega,k}$, $n_{a,k}$, and $n_{ba,k}$ describe noise vectors with zero mean (Gaussian distribution) and $C_{\omega,k}$, $C_{a,k}$, $C_{b\omega,k}$, and $C_{ba,k}$ covariance matrices. Using (17) and (18), define the state vector x_k :

$$x_k = [q_k^\top \ p_k^\top \ v_k^\top \ b_{\omega,k}^\top \ b_{a,k}^\top]^\top \in \mathbb{R}^{m_x} \quad (19)$$

with $m_x = 16$ being the state dimension. Let us introduce the augmented and additive noise vectors as follows:

$$\begin{cases} n_{x,k} = [n_{\omega,k}^\top \ n_{a,k}^\top]^\top \in \mathbb{R}^{m_{nx}} \\ n_{w,k} = [0_{10 \times 1}^\top \ n_{b\omega,k}^\top \ n_{ba,k}^\top]^\top \in \mathbb{R}^{m_{nw}} \end{cases} \quad (20)$$

where $m_{nx} = 6$ and $m_{nw} = 16$. Let u_k be input vector at time step k :

$$u_k = [\omega_{m,k}^\top \ a_{m,k}^\top]^\top \in \mathbb{R}^{m_u} \quad (21)$$

with $m_u = 6$. Let the augmented state vector be defined as:

$$x_k^a = [x_k^\top \ n_{x,k}^\top]^\top \in \mathbb{R}^{m_a} \quad (22)$$

with $m_a = m_x + m_{nx}$. In view of (17), (18), (20), (21), and (22), the overall discrete system kinematics is described by

$$x_k = f(x_{k-1}^{(i)a}, u_{k-1}) + n_{w,k-1} \quad (23)$$

with $f(\cdot) : \mathbb{R}^{m_a} \times \mathbb{R}^{m_u} \rightarrow \mathbb{R}^{m_x}$ being the state transition matrix.

Camera data: Consider $f_{w,i} \in \mathbb{R}^3$ to represent the coordinates of i th landmark point (feature) in $\{\mathcal{W}\}$ extracted via a series of stereo camera observations at the k th time step. Let $f_{b,i} \in \mathbb{R}^3$ denote the i th landmark coordinates in $\{\mathcal{B}\}$ found by triangulating [19] the features in the stereo images obtained at time step k . These vectors are related to each other as follows [3]:

$$f_{b,i} = R_q(q_k)^\top (f_{w,i} - p_k) + n_{f,i} \in \mathbb{R}^3 \quad (24)$$

with $n_{f,i}$ being Gaussian white noise related to each landmark measurement for all $i \in \{1, 2, \dots, m_f\}$ and m_f being the total number of landmarks detected at the k th sample time. It is

worth noting that landmark points vary among images captured at different k th sample time. Let us define the following relations:

$$\begin{cases} f_b = [f_{b,1}^\top \ f_{b,2}^\top \ \cdots \ f_{b,m_f}^\top]^\top \in \mathbb{R}^{3m_f} \\ f_w = [f_{w,1}^\top \ f_{w,2}^\top \ \cdots \ f_{w,m_f}^\top]^\top \in \mathbb{R}^{3m_f} \\ n_f = [n_{f,1}^\top \ n_{f,2}^\top \ \cdots \ n_{f,m_f}^\top]^\top \in \mathbb{R}^{3m_f} \end{cases} \quad (25)$$

From (25), the expression in (24) can be reformulated as follows:

$$f_{b,k} = z_k = h(x_k, f_w) + n_{f,k} \in \mathbb{R}^{m_z} \quad (26)$$

where

$$n_f \sim N(0, C_f \in \mathbb{R}^{m_z \times m_z}) \quad (27)$$

Note that $m_z = 3m_f$.

IV. QUPF-VIN DESIGN

In this section, the objective is to develop a quaternion-based unscented particle filter tailored for visual-inertial navigation and applicable to vehicles travelling in GPS-denied regions. The QUPF-VIN is based on the UKF [15], modified to operate within the \mathbb{S}^3 space and effectively manage the reduced dimensionality of quaternions. Fig. 1 provides an illustrative diagram of the proposed QUPF-VIN approach.

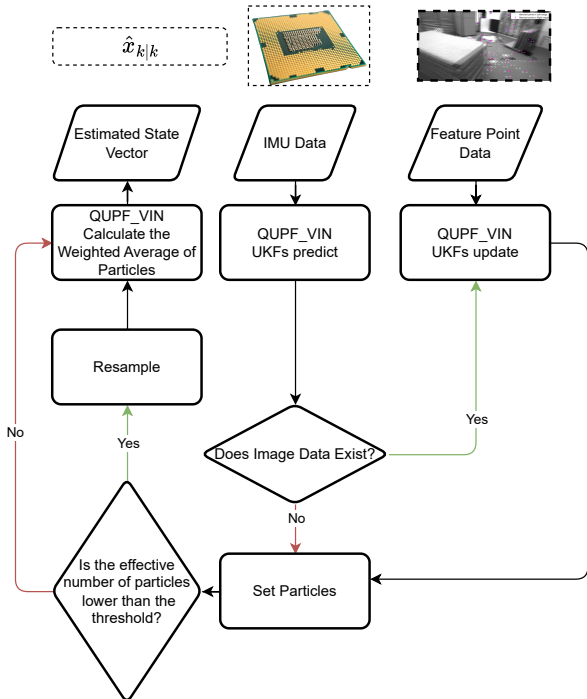


Fig. 1: Illustrative diagram of QUPF-VIN implementation algorithm.

A. QUPF-VIN Initialization

Step 1. Initialization: QUPF-VIN initialization relies on assigning an initial state estimate $\hat{x}_{0|0} = [\hat{x}_{0|0,q}^\top, \hat{x}_{0|0,-}^\top]^\top \in \mathbb{R}^{m_x}$ and covariance matrix $P_{0|0}$. $\hat{x}_{0|0,q} \in \mathbb{S}^3$ and $\hat{x}_{0|0,-} \in \mathbb{R}^{m_x-4}$ refer to quaternion and non-quaternion components, respectively. As straightforward quaternion subtraction is not feasible, the custom quaternion subtraction presented in (11) is utilized to enable quaternion subtraction. Consider the following initialization:

$$\begin{cases} \hat{x}_{0|0} = [\hat{x}_{0|0,q}^\top, \hat{x}_{0|0,-}^\top]^\top \in \mathbb{R}^{m_x} \\ P_{0|0} = \text{diag}(P_{\hat{x}_{0|0,q}}, P_{0|0,-}) \in \mathbb{R}^{(m_x-1) \times (m_x-1)} \end{cases} \quad (28)$$

where $P_{0|0,q} \in \mathbb{R}^{3 \times 3}$ and $P_{0|0,-} \in \mathbb{R}^{(m_x-4) \times (m_x-4)}$.

Step 2. Particle initialization: Given the initial covariance and state estimates in (28), m_p particles are conventionally drawn as:

$$\mathcal{X}_0^{(i)} \sim \mathcal{N}(\hat{x}_{0|0}, P_{0|0}), \quad i = \{1, 2, \dots, m_p\} \quad (29)$$

However, the dimensions of $\hat{x}_{0|0}$, and $P_{0|0}$ are not compatible (see (28)). Define the following functions $x^{q2r}(\cdot) : \mathbb{R}^{m_x} \rightarrow \mathbb{R}^{m_x-1}$ and $x^{r2q}(\cdot) : \mathbb{R}^{m_x-1} \rightarrow \mathbb{R}^{m_x}$ such that

$$x^{q2r} \left(\begin{bmatrix} x_q \\ x_- \end{bmatrix} \right) = \begin{bmatrix} x_r \\ x_- \end{bmatrix} = \begin{bmatrix} r_q(x_q) \\ x_- \end{bmatrix} \in \mathbb{R}^{m_x-1} \quad (30)$$

$$x^{r2q} \left(\begin{bmatrix} x_r \\ x_- \end{bmatrix} \right) = \begin{bmatrix} x_q \\ x_- \end{bmatrix} = \begin{bmatrix} q_r(x_r) \\ x_- \end{bmatrix} \in \mathbb{R}^{m_x} \quad (31)$$

where $x_q \in \mathbb{S}^3$, $x_r \in \mathbb{R}^3$, and $x_- \in \mathbb{R}^{m_x-4}$. Hence, the expression in (29) is re-described as follows:

$$\begin{cases} \tilde{\mathcal{X}}_0^{(i)} \sim \mathcal{N}(x^{q2r}(\hat{x}_{0|0}), P_{0|0}) & i = \{1, 2, \dots, m_p\} \\ \mathcal{X}_0^{(i)} = x^{r2q}(\tilde{\mathcal{X}}_0^{(i)}) & i = \{1, 2, \dots, m_p\} \end{cases} \quad (32)$$

where $\tilde{\mathcal{X}}_0^{(i)} \in \mathbb{R}^{m_x-1}$ and $\mathcal{X}_0^{(i)} \in \mathbb{R}^{m_x}$. The weights $w_0^{(i)}$ corresponding to each particle are initialized as $\frac{1}{m_p}$, representing equal confidence in all particles. The sigma points mean $\hat{x}_{0|0}^{(i)}$ and covariance $P_{0|0}^{(i)}$ of each particle are then initialized as:

$$\begin{cases} \hat{x}_{0|0}^{(i)} = \mathcal{X}_0^{(i)}, & i = \{1, 2, \dots, m_p\} \\ P_{0|0}^{(i)} = P_{0|0}, & i = \{1, 2, \dots, m_p\} \end{cases} \quad (33)$$

B. Prediction

Step 3. Augmentation: For every $i = \{1, 2, \dots, m_p\}$, the mean and covariance estimates are augmented to capture non-additive noise such that:

$$\hat{x}_{k-1|k-1}^{(i)a} = [\hat{x}_{k-1|k-1}^{(i)\top}, 0_{m_{n_x} \times 1}]^\top \in \mathbb{R}^{m_a} \quad (34)$$

$$P_{k-1|k-1}^{(i)a} = \text{diag}(P_{k-1|k-1}^{(i)}, C_{x,k}) \in \mathbb{R}^{(m_a-1) \times (m_a-1)} \quad (35)$$

where $\hat{x}_{k-1|k-1}^{(i)a}$ and $P_{k-1|k-1}^{(i)a}$ represent the augmented expected value and covariance matrix of each particle, respectively. The matrix $C_{x,k}$ representing the covariance matrix of n_x is defined by:

$$C_{x,k} = \text{diag}(C_{\omega,k}, C_{a,k}) \in \mathbb{R}^{m_{n_x} \times m_{n_x}} \quad (36)$$

Step 4. Sigma Point Calculations: Consider $\delta\hat{x}_{k-1,j}^{(i)a} := \left(\sqrt{(m_a - 1 + \lambda)P_{k-1|k-1}^{(i)a}}\right)_j \in \mathbb{R}^{m_a-1}$ with $\lambda \in \mathbb{R}$ being a tuning parameter. It is possible to divide $\hat{x}_{k-1|k-1}^{(i)a}$ and $\delta\hat{x}_{k-1,j}^{(i)a}$ into their attitude and non-attitude parts $\hat{x}_{k-1|k-1,q}^{(i)a} \in \mathbb{S}^3$, $\delta\hat{x}_{k-1,j,r}^{(i)a} \in \mathbb{R}^3$, and $\hat{x}_{k-1|k-1,-}^{(i)a} \in \mathbb{R}^{m_a-4}$, $\delta\hat{x}_{k-1,j,-}^{(i)a} \in \mathbb{R}^{m_a-4}$, as outlined below:

$$\begin{cases} \hat{x}_{k-1|k-1}^{(i)a} = \left[(\hat{x}_{k-1|k-1,q}^{(i)a})^\top, (\hat{x}_{k-1|k-1,-}^{(i)a})^\top \right]^\top \\ \delta\hat{x}_{k-1,j}^{(i)a} = \left[(\delta\hat{x}_{k-1,j,r}^{(i)a})^\top, (\delta\hat{x}_{k-1,j,-}^{(i)a})^\top \right]^\top \end{cases} \quad (37)$$

In the light of (12), (13), and (37), the sigma points of the i th UKF of QUPF-VIN are found by:

$$\begin{cases} \mathcal{X}_{k-1|k-1,0}^{(i)a} = \hat{x}_{k-1|k-1}^{(i)a} \in \mathbb{R}^{m_a} \\ \mathcal{X}_{k-1|k-1,j}^{(i)a} = \hat{x}_{k-1|k-1}^{(i)a} \oplus \delta\hat{x}_j^{(i)a} \\ \quad = \left[\hat{x}_{k-1|k-1,q}^{(i)a} \oplus \delta\hat{x}_{k-1,j,r}^{(i)a}, \hat{x}_{k-1|k-1,-}^{(i)a} + \delta\hat{x}_{k-1,j,-}^{(i)a} \right] \in \mathbb{R}^{m_a} \\ \mathcal{X}_{k-1|k-1,j+m_a}^{(i)a} = \hat{x}_{k-1|k-1}^{(i)a} \ominus \delta\hat{x}_j^{(i)a} \\ \quad = \left[\hat{x}_{k-1|k-1,q}^{(i)a} \ominus \delta\hat{x}_{k-1,j,r}^{(i)a}, \hat{x}_{k-1|k-1,-}^{(i)a} - \delta\hat{x}_{k-1,j,-}^{(i)a} \right] \in \mathbb{R}^{m_a}, \\ \quad j = \{1, 2, \dots, 2(m_a - 1)\} \end{cases} \quad (38)$$

Step 5. Propagation: Given IMU measurements, each sigma point for each UKF is propagated through the state transition function (23) to find predicted sigma points $\mathcal{X}_{k|k-1,j}^{(i)}$. This can be shown as:

$$\mathcal{X}_{k|k-1,j}^{(i)} = f(\mathcal{X}_{k-1|k-1,j}^{(i)a}, u_{k-1}) \in \mathbb{R}^{m_x} \quad (39)$$

Using the propagated sigma points, the mean $\hat{x}_{k|k-1}^{(i)}$ and covariance matrix $P_{k|k-1}^{(i)}$ for each UKF should be computed. Consider:

$$\hat{x}_{k|k-1}^{(i)} = \left[\hat{x}_{k|k-1,q}^{(i)\top} \quad \hat{x}_{k|k-1,-}^{(i)\top} \right]^\top \in \mathbb{R}^{m_x} \quad (40)$$

$$\mathcal{X}_{k|k-1,j}^{(i)} = \left[\mathcal{X}_{k|k-1,q}^{(i)\top} \quad \mathcal{X}_{k|k-1,-}^{(i)\top} \right]^\top \in \mathbb{R}^{m_x} \quad (41)$$

where $\hat{x}_{k|k-1,q}^{(i)}, \mathcal{X}_{k|k-1,q}^{(i)} \in \mathbb{S}^3$, and $\hat{x}_{k|k-1,-}^{(i)}, \mathcal{X}_{k|k-1,-}^{(i)} \in \mathbb{R}^{m_x-4}$. Thereby, one has

$$\hat{x}_{k|k-1}^{(i)} = \left[\text{QWA}(\{\mathcal{X}_{k|k-1,j,q}^{(i)}\}, \{w_j^m\}) \right. \\ \left. \sum_{j=0}^{2(m_a-1)} w_j^m \mathcal{X}_{k|k-1,j,-}^{(i)} \right] \in \mathbb{R}^{m_x} \quad (42)$$

$$P_{k|k-1}^{(i)} = \sum_{j=0}^{2(m_a-1)} w_j^c \left(\mathcal{X}_{k|k-1,j}^{(i)} \ominus \hat{x}_{k|k-1}^{(i)} \right) \left(\mathcal{X}_{k|k-1,j}^{(i)} \ominus \hat{x}_{k|k-1}^{(i)} \right)^\top \\ + C_{w,k} \in \mathbb{R}^{(m_x-1) \times (m_x-1)} \quad (43)$$

where

$$C_{w,k} = \begin{bmatrix} 0_{9 \times 9} & 0_{3 \times 3} & 0_{3 \times 3} \\ 0_{9 \times 9} & C_{b\omega,k} & 0_{3 \times 3} \\ 0_{9 \times 9} & 0_{3 \times 3} & C_{ba,k} \end{bmatrix} \in \mathbb{R}^{(m_{n_w}-1) \times (m_{n_w}-1)} \quad (44)$$

Considering (11), the subtraction in (43) is obtained by:

$$\mathcal{X}_{k|k-1,j}^{(i)} \ominus \hat{x}_{k|k-1}^{(i)} = \begin{bmatrix} \mathcal{X}_{k|k-1,j,q}^{(i)} \ominus \hat{x}_{k|k-1,q}^{(i)} \\ \mathcal{X}_{k|k-1,j,-}^{(i)} - \hat{x}_{k|k-1,-}^{(i)} \end{bmatrix} \in \mathbb{R}^{m_x-1} \quad (45)$$

Note that the weights w_j^m and w_j^c in (42) and (43) are found by:

$$\begin{cases} w_0^m = \frac{\lambda}{\lambda + (m_a - 1)} \in \mathbb{R} \\ w_0^c = \frac{\lambda}{\lambda + (m_a - 1)} + 1 - \alpha^2 + \beta \in \mathbb{R} \\ w_j^m = w_j^c = \frac{1}{2((m_a - 1) + \lambda)} \in \mathbb{R} \\ \quad j = \{1, \dots, 2(m_a - 1)\} \end{cases} \quad (46)$$

with $\alpha, \beta \in \mathbb{R}$ being tuning parameters.

C. Update

Step 6. Predict Measurement: Every sigma point is passed through the measurement function (26) to predict the measurement vector. The measurement sigma points $\mathcal{Z}_{k|k-1,j}^{(i)}$ are obtained as follows:

$$\mathcal{Z}_{k|k-1,j}^{(i)} = h(\mathcal{X}_{k|k-1,j}^{(i)}, f_w) \in \mathbb{R}^{m_z} \quad (47)$$

The covariance matrices $P_{z_k, z_k}^{(i)} \in \mathbb{R}^{m_z \times m_z}$ and $P_{x_k, z_k}^{(i)} \in \mathbb{R}^{(m_x-1) \times m_z}$ and the mean estimated measurement vector $\hat{z}_{k|k-1}^{(i)} \in \mathbb{R}^{m_z}$ for each UKF are found by:

$$\hat{z}_{k|k-1}^{(i)} = \sum_{j=0}^{2(m_a-1)} w_j^m \mathcal{Z}_{k|k-1,j}^{(i)} \quad (48)$$

$$P_{z_k, z_k}^{(i)} = \sum_{j=0}^{2(m_a-1)} w_j^c [\mathcal{Z}_{k|k-1,j}^{(i)} - \hat{z}_{k|k-1}^{(i)}][\mathcal{Z}_{k|k-1,j}^{(i)} - \hat{z}_{k|k-1}^{(i)}]^\top \\ + C_f \quad (49)$$

$$P_{x_k, z_k}^{(i)} = \sum_{j=0}^{2(m_a-1)} w_j^c [\mathcal{X}_{k|k-1,j}^{(i)} \ominus \hat{x}_{k|k-1}^{(i)}][\mathcal{Z}_{k|k-1,j}^{(i)} - \hat{z}_{k|k-1}^{(i)}]^\top \quad (50)$$

The \ominus operator in (50) follows the map in (45). The Kalman gains $K_k^{(i)}$, estimation covariance matrices $P_{k|k}^{(i)}$ and correction vectors $\delta\hat{x}_{k|k-1}^{(i)}$ are defined by:

$$K_k^{(i)} = P_{x_k, z_k}^{(i)} P_{z_k, z_k}^{(i)\top} \in \mathbb{R}^{(m_x-1) \times m_z} \quad (51)$$

$$P_{k|k}^{(i)} = P_{k|k-1}^{(i)} - K_k^{(i)} P_{z_k, z_k}^{(i)} K_k^{(i)\top} \in \mathbb{R}^{(m_x-1) \times (m_x-1)} \quad (52)$$

$$\delta\hat{x}_{k|k-1}^{(i)} := K_k^{(i)} (z_k - \hat{z}_{k|k-1}^{(i)}) \in \mathbb{R}^{m_x-1} \quad (53)$$

Let us divide $\delta\hat{x}_{k|k-1}^{(i)}$ into its attitude ($\delta\hat{x}_{k|k-1,r}^{(i)} \in \mathbb{R}^3$) and non-attitude ($\delta\hat{x}_{k|k-1,-}^{(i)} \in \mathbb{R}^{m_x-4}$) components:

$$\delta\hat{x}_{k|k-1}^{(i)} = \left[\delta\hat{x}_{k|k-1,r}^{(i)\top} \quad \delta\hat{x}_{k|k-1,-}^{(i)\top} \right]^\top \quad (54)$$

Then, the estimated state vector for each UKF $\hat{x}_{k|k}^{(i)}$ is defined by:

$$\hat{x}_{k|k}^{(i)} = \hat{x}_{k|k-1}^{(i)} \oplus \delta\hat{x}_{k|k-1}^{(i)} \quad (55)$$

where

$$\hat{x}_{k|k-1}^{(i)} \oplus \delta\hat{x}_{k|k-1}^{(i)} = \begin{bmatrix} \hat{x}_{k|k-1,q}^{(i)} \oplus \delta\hat{x}_{k|k-1,r}^{(i)} \\ \hat{x}_{k|k-1,-}^{(i)} + \delta\hat{x}_{k|k-1,-}^{(i)} \end{bmatrix} \quad (56)$$

Step 7. Particle and Weight calculations: Using the estimated vector $\hat{x}_{k|k-1}^{(i)}$ and covariance matrix $P_{k|k}^{(i)}$ as the mean and covariance matrix of a Gaussian distribution, the particles $\mathcal{X}_k^{(i)}$ are drawn similar to (32):

$$\begin{cases} \tilde{\mathcal{X}}_k^{(i)} \sim \mathcal{N}\left(x^{q2r}\left(\hat{x}_{k|k-1}^{(i)}\right), P_{k|k}^{(i)}\right) \\ \mathcal{X}_k^{(i)} = x^{r2q}(\tilde{\mathcal{X}}_k^{(i)}) \end{cases} \quad (57)$$

The weights $w_k^{(i)}$ corresponding to each particle at the current time-step represent how accurate each particle is and they are defined by:

$$\tilde{w}_k^{(i)} = \frac{\mathbb{P}\left(z_k|\mathcal{X}_k^{(i)}\right)\mathbb{P}\left(\mathcal{X}_k^{(i)}|\mathcal{X}_{k-1}^{(i)}\right)}{\mathbb{P}\left(\mathcal{X}_k^{(i)}|z_{1:k}\right) + \epsilon} \quad (58)$$

ϵ is added to avoid numerical instabilities for the case of zero weight and division by zero. The probability terms in (58) are calculated by:

$$\begin{cases} \mathbb{P}\left(z_k|\mathcal{X}_k^{(i)}\right) = \mathcal{N}\left(z_k|h\left(\mathcal{X}_k^{(i)}\right), C_f\right) \\ \mathbb{P}\left(\mathcal{X}_k^{(i)}|\mathcal{X}_{k-1}^{(i)}\right) = \mathcal{N}\left(x^{q2r}\left(\mathcal{X}_k^{(i)}\right)|x^{q2r}\left(\hat{x}_{k|k-1}^{(i)}\right), P_{k|k-1}^{(i)}\right) \\ \mathbb{P}\left(\mathcal{X}_k^{(i)}|z_{1:k}\right) = \mathcal{N}\left(x^{q2r}\left(\mathcal{X}_k^{(i)}\right)|x^{q2r}\left(\hat{x}_{k|k}^{(i)}\right), P_{k|k}^{(i)}\right) \end{cases} \quad (59)$$

Next, the weights are normalized as follows:

$$w_k^{(i)} = \frac{\tilde{w}_k^{(i)}}{\sum_{i=1}^{m_p} \tilde{w}_k^{(i)}} \quad (60)$$

Step 8. Resampling: To address the degeneracy challenging problem of particle filters, resampling is performed once the effective number of samples $m_{eff} \in \mathbb{R}$ falls below a predefined threshold $m_{thr} \in \mathbb{R}$ [20]. The effective number of samples is calculated by:

$$m_{eff} = \frac{1}{\sum \left(w_k^{(i)}\right)^2} \quad (61)$$

The particles are then resampled if m_{eff} is lower than a certain threshold m_{thr} . Consider the set $\{\mathcal{X}_k^{(i)}, P_{k|k}^{(i)}\}$ as instances of a random variable, associated with the probability set $\{w_k^{(i)}\}$. During the resampling step, m_p samples are drawn from $\{\mathcal{X}_k^{(i)}, P_{k|k}^{(i)}\}$ according to their corresponding probabilities. Note that a single particle may be sampled multiple times. After resampling, the weights are updated to reflect a uniform distribution, as the distribution is now represented by the number of particles rather than their individual weights. The resampling process is formally expressed as:

$$\left[\{\mathcal{X}_k^{(i)}, P_{k|k}^{(i)}\}, \{w_k^{(i)}\}\right] \leftarrow \text{Resample}\left(\{\mathcal{X}_k^{(i)}, P_{k|k}^{(i)}\}, \{w_k^{(i)}\}\right) \quad (62)$$

Step 9. Particles weighted average: The weighted average of the particles will be the estimated state vector at the current time step. Let us divide each particle into its quaternion $\mathcal{X}_{k,q} \in \mathbb{S}^3$ and non-quaternion $\mathcal{X}_{k,-}$ components. Hence, the estimated state vector $\hat{x}_{k|k}$ is defined by:

$$\hat{x}_{k|k} = \begin{bmatrix} \text{QWA}\left(\{\mathcal{X}_{k,q}^{(i)}\}, \{w_k^{(i)}\}\right) \\ \sum_{i=0}^{m_p} w_k^{(i)} \mathcal{X}_{k,-}^{(i)} \end{bmatrix} \in \mathbb{R}^{m_x} \quad (63)$$

The particles will also be set as the expected value of the UKFs' estimated state vectors which will be used in the next iteration at 34. In other words:

$$x_{k|k}^{(i)} = \mathcal{X}_k^{(i)}$$

Step 10. Iterate: Go back to Step 2 and iterate with $k \rightarrow k + 1$.

V. NUMERICAL RESULTS

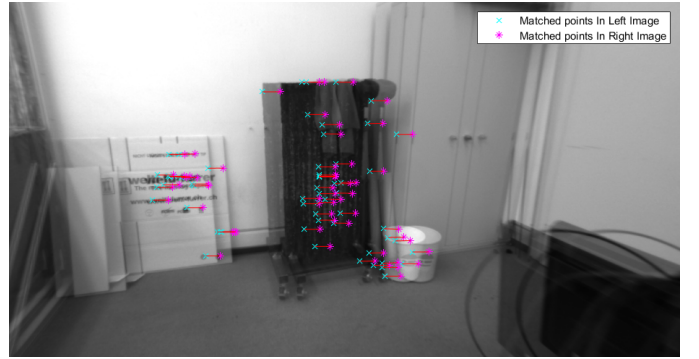


Fig. 2: A sample of matched landmark data points from left to right frame of EuRoC dataset [21].

This section evaluates the effectiveness and robustness of the proposed QUPF-VIN algorithm using a real-world dataset from a quadrotor flight in 3D space, specifically the EuRoC dataset [21]. The test platform is the Asctec Firefly hexarotor Micro Aerial Vehicle (MAV), operating in a GPS-denied indoor environment. Ground truth data, including true position and orientation (quaternion), were collected using an OptiTrack localization system. The measurements consist of 6-axis IMU data (linear acceleration and angular velocity) and stereo images. The stereo images, captured at 20 Hz, were obtained from an Aptina MT9V034 global shutter sensor, while the IMU data, including linear acceleration and angular velocity, were collected at 200 Hz using an ADIS16448 sensor. Due to the difference in sampling rates between the IMU and the camera, landmark measurements are not available for every IMU data point. To address this challenge, the proposed algorithm updates the state when image data is available. Otherwise, the particles $\mathcal{X}_k^{(i)}$ are set to the predicted state vector $\hat{x}_{k|k-1}^{(i)}$ while image data is unavailable.

For every set of stereo images, the landmark points are defined via the Kanade-Lucas-Tomasi (KLT) approach [22]. As illustrative example, the landmark matching between two instantaneous frame is presented in Fig. 2. The mapping

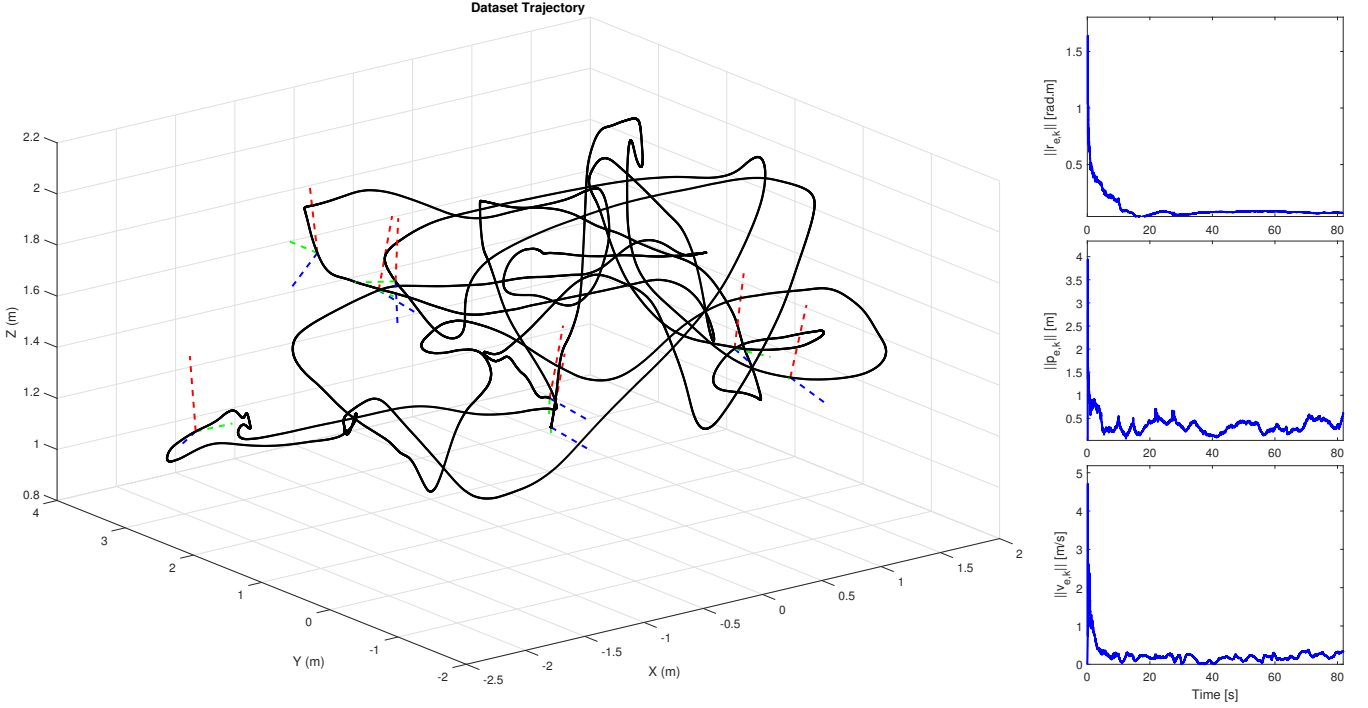


Fig. 3: Performance assessment using the EuRoC V1_02_medium dataset [21]. The left side shows UAV navigation (estimation) trajectory 3D space where the position is depicted in black solid line while the orientation is represented by red, green, and blue dashed lines. The right side presents normalized values of error vectors: orientation error $\|r_{e,k}\|$, position error $\|p_{e,k}\|$, and linear velocity error $\|v_{e,k}\|$ in blue solid lines.

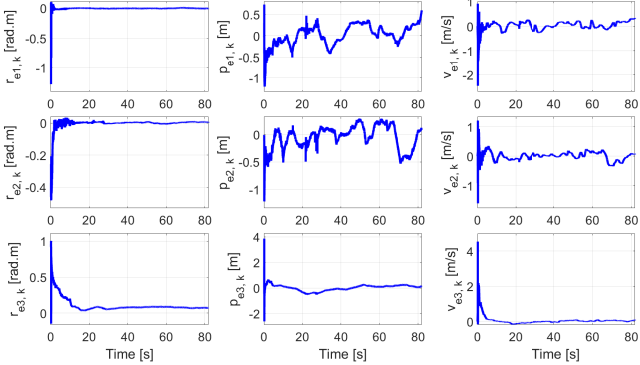


Fig. 4: Estimation error: Rotation (left portion), position (middle portion), and linear velocity (right portion).

triangulation approach in [19] were utilized to project the 2D matched points into the 3D space, describing the landmark point. The filter was also compared to the EKF, which is a commonly adopted base filter in this domain. To ensure a fair comparison, both filters were initialized with the same values and parameters. In Fig. 5 the magnitude of orientation (top), position (middle), and velocity (bottom) estimation errors are plotted against time. The EKF results are represented by solid red lines, while the QUPF-VIN results are depicted by dashed blue lines. As shown in Fig. 5, the proposed filter outperformed the EKF in terms of accuracy and speed, specifically in reducing the magnitudes of orientation, position, and linear velocity estimation errors. The mapping $\mathbb{S}^3 \times \mathbb{S}^3 \rightarrow \mathbb{R}^3$

associated with the subtraction operator provided in (11) is used to define the orientation estimation error $r_{e,k}$ such that:

$$r_{e,k} = q_k \ominus \hat{q}_k \quad (64)$$

with $r_{e,k} = [r_{e1,k} \ r_{e2,k} \ r_{e3,k}]^\top \in \mathbb{R}^3$. Consider expressing the estimation errors of position and linear velocity at the k th sample step as follows:

$$p_{e,k} = p_k - \hat{p}_k = [p_{e1,k} \ p_{e2,k} \ p_{e3,k}]^\top \in \mathbb{R}^3 \quad (65)$$

$$v_{e,k} = v_k - \hat{v}_k = [v_{e1,k} \ v_{e2,k} \ v_{e3,k}]^\top \in \mathbb{R}^3 \quad (66)$$

Fig. 3 presents the performance of QUPF-VIN using the EuRoC V1_02_medium room dataset [21]. The left portion of Fig. 3 shows the drone's estimated position trajectory and orientation during the navigation experiment with 6 DoF. The right portion of Fig. 3 reveals the estimation errors for orientation, position, and linear velocity. As illustrated in Fig. 3, the proposed algorithm exhibits rapid error convergence to near-zero values, even when initialized with large errors, confirming the robustness and reliability of the QUPF-VIN algorithm. This confirms the robustness and reliability of the proposed QUPF-VIN algorithm. To further evaluate the filter's performance, Fig. 4 plots each component of the orientation, position, and linear velocity estimation errors over time, demonstrating consistent convergence across all dimensions.

Additionally, the filter was compared to the EKF, a widely used baseline in this field. For a fair comparison, both filters were initialized with identical values and parameters. In Fig. 5, the magnitudes of the orientation (top), position (middle), and velocity (bottom) estimation errors are plotted against time,

with EKF results represented by solid red lines and QUPF-VIN results by dashed blue lines. As shown in Fig. 5, the proposed filter outperforms the EKF in both accuracy and speed, significantly reducing the magnitude of the orientation, position, and linear velocity estimation errors.

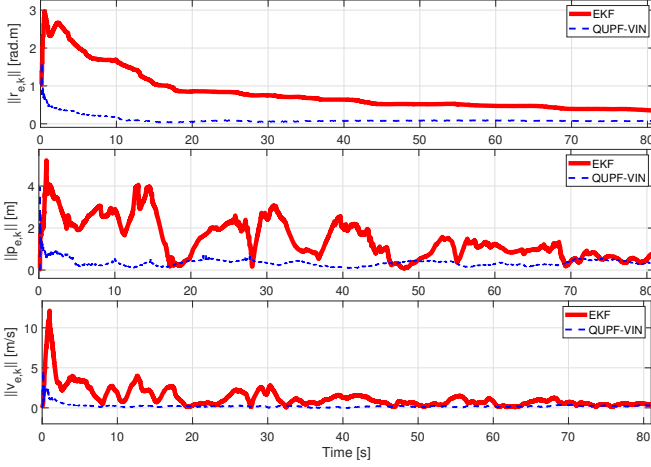


Fig. 5: Comparison results of EKF (literature in red) and the proposed QUPF-VIN (in blue).

VI. CONCLUSION

This article investigated the navigation problem of a vehicle operating with six degrees of freedom. A novel geometric Quaternion-based Unscented Particle Filter for Visual-Inertial Navigation (QUPF-VIN) has been developed to estimate the vehicle's navigation state (orientation, position, and linear velocity) while mitigating measurement uncertainties. The proposed filter effectively addressed kinematic nonlinearities and ensures computational efficiency, even at low sampling rates. The proposed algorithm has been structured using unit quaternions to accurately model true navigation kinematics and avoid singularities. The algorithm leveraged sensor fusion from a vision unit (e.g., monocular or stereo camera) and a 6-axis IMU. The performance of the QUPF-VIN was evaluated using a real-world dataset of an indoor drone flight, which included stereo camera images and IMU data collected at a low sampling rate. The results demonstrated good navigation performance, with tracking errors approaching zero. Furthermore, the proposed filter outperformed a baseline EKF in comparison.

REFERENCES

- [1] H. A. Hashim, "Advances in UAV Avionics Systems Architecture, Classification and Integration: A Comprehensive Review and Future Perspectives," *Results in Engineering*, vol. 25, p. 103786, 2025.
- [2] D. P. Koch and et al., "Relative multiplicative extended kalman filter for observable gps-denied navigation," *The International Journal of Robotics Research*, vol. 39, no. 9, pp. 1085–1121, 2020.
- [3] H. A. Hashim, M. Abouheaf, and M. A. Abido, "Geometric stochastic filter with guaranteed performance for autonomous navigation based on imu and feature sensor fusion," *Control Engineering Practice*, vol. 116, p. 104926, 2021.
- [4] H. A. Hashim, L. J. Brown, and K. McIsaac, "Nonlinear pose filters on the special euclidean group se (3) with guaranteed transient and steady-state performance," *IEEE Transactions on Systems, Man, and Cybernetics: Systems*, vol. 51, no. 5, pp. 2949–2962, 2019.
- [5] H. A. Hashim, "Gps-denied navigation: Attitude, position, linear velocity, and gravity estimation with nonlinear stochastic observer," in *2021 American Control Conference (ACC)*. IEEE, 2021, pp. 1149–1154.
- [6] H. A. Hashim, L. J. Brown, and K. McIsaac, "Nonlinear stochastic attitude filters on the special orthogonal group 3: Ito and stratonovich," *IEEE Transactions on Systems, Man, and Cybernetics: Systems*, vol. 49, no. 9, pp. 1853–1865, 2018.
- [7] H. A. Hashim and F. L. Lewis, "Nonlinear stochastic estimators on the special euclidean group se (3) using uncertain imu and vision measurements," *IEEE Transactions on Systems, Man, and Cybernetics: Systems*, vol. 51, no. 12, pp. 7587–7600, 2020.
- [8] J. F. Vasconcelos, B. Cardeira, C. Silvestre, P. Oliveira, and P. Batista, "Discrete-time complementary filters for attitude and position estimation: Design, analysis and experimental validation," *IEEE Transactions on Control Systems Technology*, vol. 19, no. 1, pp. 181–198, 2010.
- [9] A. Fornasier, Y. Ng, R. Mahony, and S. Weiss, "Equivariant filter design for inertial navigation systems with input measurement biases," in *2022 International Conference on Robotics and Automation (ICRA)*. IEEE, 2022, pp. 4333–4339.
- [10] H. A. Hashim, A. E. Eltoukhy, and K. G. Vamvoudakis, "Uwb ranging and imu data fusion: Overview and nonlinear stochastic filter for inertial navigation," *IEEE Transactions on Intelligent Transportation Systems*, 2023.
- [11] J. Ali and M. Ushaq, "A consistent and robust kalman filter design for in-motion alignment of inertial navigation system," *Measurement*, vol. 42, no. 4, pp. 577–582, 2009.
- [12] K. Sun and et al., "Robust stereo visual inertial odometry for fast autonomous flight," *IEEE Robotics and Automation Letters*, vol. 3, no. 2, pp. 965–972, 2018.
- [13] T. Cantelobre, C. Chahbazian, A. Croux, and S. Bonnabel, "A real-time unscented kalman filter on manifolds for challenging auv navigation," in *2020 IEEE/RSJ International Conference on Intelligent Robots and Systems (IROS)*. IEEE, 2020, pp. 2309–2316.
- [14] K. Hong, S. Kim, J. Park, and H. Bang, "Particle filter approach to vision-based navigation with aerial image segmentation," *Journal of Aerospace Information Systems*, vol. 18, no. 12, pp. 964–972, 2021.
- [15] R. Van Der Merwe, A. Doucet, N. De Freitas, and E. Wan, "The unscented particle filter," *Advances in neural information processing systems*, vol. 13, 2000.
- [16] H. A. Hashim, "Special orthogonal group SO(3), euler angles, angle-axis, rodriguez vector and unit-quaternion: Overview, mapping and challenges," *arXiv preprint arXiv:1909.06669*, 2019.
- [17] H. A. Hashim, A. E. Eltoukhy, K. G. Vamvoudakis, and M. I. Abouheaf, "Nonlinear deterministic observer for inertial navigation using ultra-wideband and IMU sensor fusion," in *2023 IEEE/RSJ International Conference on Intelligent Robots and Systems (IROS)*. IEEE, 2023, pp. 3085–3090.
- [18] H. A. Hashim, "Exponentially stable observer-based controller for vtol-uavs without velocity measurements," *International Journal of Control*, vol. 96, no. 8, pp. 1946–1960, 2023.
- [19] R. Hartley and A. Zisserman, *Multiple view geometry in computer vision*. Cambridge university press, 2003.
- [20] X. Fu and Y. Jia, "An improvement on resampling algorithm of particle filters," *IEEE Transactions on Signal Processing*, vol. 58, no. 10, pp. 5414–5420, 2010.
- [21] M. Burri, J. Nikolic, P. Gohl, T. Schneider, J. Rehder, S. Omari, M. W. Achtelik, and R. Siegwart, "The EuRoC micro aerial vehicle datasets," *The International Journal of Robotics Research*, vol. 35, no. 10, pp. 1157–1163, 2016.
- [22] J. Shi and Tomasi, "Good features to track," in *1994 Proceedings of IEEE Conference on Computer Vision and Pattern Recognition*, 1994, pp. 593–600.